RSC Advances

ROYAL SOCIETY OF CHEMISTRY

www.rsc.org/advances

Graphical Abstract

Ruthenium oxide-based nanocomposites with high specific surface area and improved capacitance as a supercapacitor

Pengfei Wang[a,b], Hui Liu[a], Qiangqiang Tan[a,*], and Jun Yang[a,*]

[a] State Key Laboratory of Multiphase Complex Systems, Institute of Process Engineering, Chinese Academy of Sciences, Beijing, China 100190. Tel.: 86-10-6252 9377; Fax: 86-10-8254 5008; E-mail: qtan@ipe.ac.cn (Q.T.); Fax: 86-10-8254 4814; Tel: 86-10-8254 4915; E-mail: jyang@ipe.ac.cn (J.Y.)

[b] University of Chinese Academy of Sciences, No. 19A Yuquan Road, Beijing, 100049, China

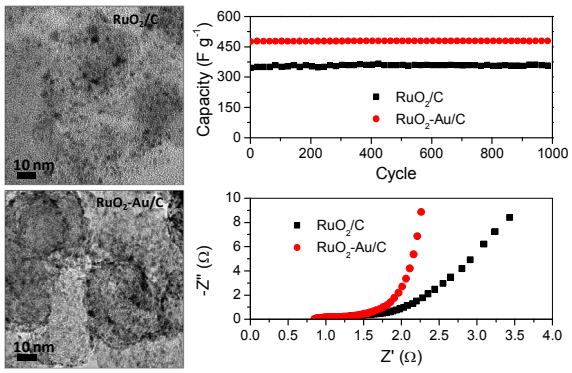

A solvothermal approach and a mutual oxidation-reduction strategy were demonstrated for the synthesis of RuO_2-based nanocomposites for supercapacitors.

Cite this: DOI: 10.1039/c0xx00000x

www.rsc.org/xxxxxx

ARTICLE TYPE

Ruthenium oxide-based nanocomposites with high specific surface area and improved capacitance as a supercapacitor†

Pengfei Wang,[ab] HuiLiu,[a] Qiangqiang Tan[c]* and Jun Yang[a]*

Received (in XXX, XXX) Xth XXXXXXXXX 20XX, Accepted Xth XXXXXXXXX 20XX

DOI: 10.1039/b000000x

A solvothermal strategy and a mutual oxidation-reduction approach are used to fabricate ruthenium oxide (RuO_2)-based nanocomposites, including RuO_2 and RuO_2-gold (Au) nanoparticles supported on commercial carbon supports (RuO_2/C and RuO_2-Au/C nanocomposites). The novelty of this work lies in the synthetic approaches, which are based on a thermal decomposition of metal complexes formed by $RuCl_3$ and dodecylamine at room temperature (for RuO_2/C) and the mutual oxidation-reduction phenomenon between $RuCl_3$ and $HAuCl_4$ at elevated temperature (for RuO_2-Au/C) in the presence of carbon supports. In particular, the as-prepared RuO_2/C and RuO_2-Au/C nanocomposites for supercapacitor adopting the H_2SO_4 electrolyte exhibit high specific capacitances of 537.7 F g^{-1} and 558.2 F g^{-1}, respectively, at a current density of 50 mA g^{-1}. The specific capacitance maintains 350.1 F g^{-1} for RuO_2/C nanocomposites and 478.5 F g^{-1} for RuO_2-Au/C nanocomposites at current density of 200 mA g^{-1} with good cycling stability. The comparison of the electrochemical measurements of RuO_2/C and RuO_2-Au/C nanocomposites demonstrates that the presence of Au in the nanocomposites is favorable for the enhancement in capacitive behavior of RuO_2.

1 Introduction

An increasing interest has been devoted towards the development of nanocomposites consisting of two or more different classes of materials with solid-state interfaces.[1–14] The composite structures can combine two or more functionalities in one unit and oftentimes exhibit synergistically enhanced properties compared to the simple sum of the constituents.[15–24] For example, the Pt nanoparticles in Pt-Fe_3O_4 dumbbell-like structures, which were synthesized by epitaxial growth of Fe onto Pt nanoparticles followed by Fe oxidation, show a 20-fold increase in mass activity toward oxygen reduction reaction compared with the single component Pt nanoparticles and the commercial 3 nm Pt particles due to the electronic coupling between Pt and Fe_3O_4 in Pt-Fe_3O_4 dumbbell-like particles, which leads to slight change in electronic structure of Pt and results in significant improvement in Pt catalysis.[25] In addition, in core-shell structured CdSe-Pt nanocomposites obtained by reducing platinum precursors with sodium citrate in the presence of previously formed CdSe nanocrystals, the compressive strain effect imposed from the CdSe core on the deposited Pt shell results in an appropriate downshift of the d band center of Pt catalysts, which leads to the enhancement of the core-shell structured nanocomposites for catalyzing the oxygen reduction reaction and methanol oxidation reaction in direct methanol fuel cells.[26]

Seed-mediated growth, where the metal precursors are reduced directly on the surface of pre-made nanoparticles, is the most common approach for the synthesis of nanocomposites.[1–4,12,16–19] In this strategy, the formation and morphology of the final composite products are largely affected by a number of variables, e.g. lattice constants of constituent materials and their interfacial energy, size of the seeds, concentration and ratio of second material precursors to the seed nanoparticles, and the surface chemistry of the seeds, which complicate the synthesis of the nanocomposites. Considering the continuous exploration of the properties and consequent applications of the composite nanostructures, the development of effective approaches for the production of nanocomposites would be undoubtedly important and pose significant challenges.

Herein, we demonstrate a solvothermal strategy and a mutual oxidation-reduction approach for the fabrication of RuO_2-based nanocomposites, including RuO_2 and RuO_2-Au supported on commercial carbon supports (RuO_2/C and RuO_2-Au/C nanocomposites). The novelty of this work lies in the synthetic approaches, which are based on a thermal decomposition of metal complexes formed by $RuCl_3$ and dodecylamine at room temperature (for RuO_2/C) and the mutual oxidation-reduction phenomenon between $RuCl_3$ and $HAuCl_4$ at elevated temperature (for RuO_2-Au/C) in the presence of carbon supports. We will demonstrate that the final RuO_2/C and RuO_2-Au/C nanocomposites have high specific surface area and improved capacitance as a supercapacitor. Considering the remarkable simplicity of the synthetic approaches, the studies in this work might be promising for creating RuO_2-based nanocomposites on a large scale for application in electrochemical capacitors.

2 Experimental

2.1 General materials

The chemical reagents, including ruthenium(III) chloride ($RuCl_3$, Ru content 45~55%), hydrogen tetrachloroaurate(III) trihydrate ($HAuCl_4 \cdot 3H_2O$, 99.9%), dodecylamine (DDA, 98%), Nafion 117 solution (5% in a mixture of lower aliphatic alcohols and water) from Aladdin Reagents, ethanol (99%) and toluene (99.5%) from Beijing Chemical Works, and Vulcan XC-72 carbon powders (XC-72C, BET surface area = 250 m^2 g^{-1} and average particle size = 40~50 nm) from Cabot Corporation, were used as received. Deionized water was distilled by a Milli-Q Ultrapure-water purification system. All glassware and Teflon-coated magnetic stir bars were cleaned with *aqua regia*, followed by copious washing with de-ionized water before drying in an oven.

2.2 Synthesis of RuO_2/C and RuO_2-Au/C nanocomposites

RuO_2/C nanocomposites were prepared by a solvothermal approach. Typically, 25 mg of $RuCl_3$ was dissolved into 60 mL of DI water with vigorous stirring. Meanwhile, 4.8 mL of DDA was dissolved into 120 mL of ethanol. The two solutions were mixed together under continuous stirring. The mixture was transferred into a 100-mL Teflon-lined stainless steel autoclave, which was then heated at 160°C for 12 h under vigorous stirring. After cooling down to room temperature, the RuO_2 products were collected by centrifugation, washed twice with ethanol, and dispersed into 30 mL of toluene. Subsequently, 60 mg of XC-72C was added into toluene colloidal solution of the RuO_2 product. After aging for 4 h under continuous stirring, the RuO_2/C nanocomposites were recovered by centrifugation, and dried at room temperature in vacuum.

For the preparation of RuO_2-Au/C nanocomposites, 60 mL of 2 mM aqueous $RuCl_3$ solution, 20 mL of 2 mM aqueous $HAuCl_4$ solution, and 60 mg of XC-72C were mixed together. The mixture was refluxed at 110°C (temperature of oil bath) for 5 min under stirring. Subsequently, the mixture was cool down and aged at room temperature for 4 h under continuous stirring. Precipitates thus formed were collected by centrifugation and washed with DI water thrice to remove the water-soluble ions (ions formed in the process i.e. H^+ and Cl^-). The RuO_2-Au/C nanocomposites as-obtained were then dried at room temperature in vacuum.

2.3 Characterization of RuO_2/C and RuO_2-Au/C nanocomposites

Transmission electron microscopy (TEM) and high resolution TEM (HRTEM) were performed on the JEOL JEM-2100 electron microscope operating at 200 kV with a supplied software for automated electron tomography. For the TEM measurements, a drop of the nanoparticle solution was dispensed onto a 3-mm carbon-coated copper grid. Excessive solution was removed by an absorbent paper, and the sample was dried under vacuum at room temperature. An energy dispersive X-ray spectroscopy (EDX) analyzer attached to the TEM was used to analyze the chemical compositions of the synthesized nanoparticles. X-ray photoelectron spectroscopy (XPS) was conducted on a VG ESCALAB MKII spectrometer. Powder X-ray diffraction (XRD) patterns were recorded on a Rigaku D/Max-3B diffractometer, using Cu Kα radiation (λ = 1.54056 Å).

2.4 Fabrication of electrode and electrochemical measurements

The working electrodes were fabricated by mixing the as-prepared RuO_2/C or RuO_2-Au/C powders, carbon black, and polytetrafluoroethylene (PTFE) with a mass ratio of 85:10:5 and then dispersing in small amount of ethanol for the formation of paste, which was pressed into tablets and dried at 100°C for 10 h in vacuum. Subsequently, the tablets were coated onto the titanium mesh under the pressure of 10 MPa to obtain the electrode. The mass of as-prepared nanocomposites coated on the titanium mesh was 2 mg.

All of the electrochemical measurements were carried out using a two electrode setup: the titanium mesh that coated with RuO_2/C or RuO_2-Au/C nanocomposites was used as the working electrode. The measurements were performed in a 1 M aqueous H_2SO_4 electrolyte at room temperature. Cyclic voltammetry (CV), galvanostatic charge/discharge test, and electrochemical impedance spectroscopy (EIS) measurements were obtained using a CHI650 electrochemical workstation. CV tests were done between -1.0 and 1.0 V at scan rates of 5, 10, 20, 50, and 100 mV s^{-1}. EIS measurements were conducted over the frequency range from 100 kHz to 10 mHz. The specific capacitance of the electrode can be calculated using the following equation:

$$C = \frac{It}{\Delta V m}$$

where C is the specific capacitance (F g^{-1}), I is the response current density (A g^{-1}), ΔV is the potential (V) and m is the mass of the electroactive materials in the electrodes (g).

3 Results and discussion

3.1 RuO_2/C nanocomposites

Upon mixing the aqueous solution of $RuCl_3$ and ethanolic solution of DDA, metal complexes composed of $RuCl_3$ and DDA are formed in term of $Ru(DDA)_nCl_3$.[27] Ethanol was used to ensure the sufficient contact between $RuCl_3$ and DDA since it is water-miscible and a good solvent for DDA. The $RuCl_3$-DDA metal complexes are decomposed at elevated temperature and the Ru^{3+} ions are further oxidized to Ru^{4+} by air, resulting in the generation of RuO_2 products, which subsequently grow into RuO_2 nanoparticles and are protected by DDA. After collection of the RuO_2 nanoparticles by centrifugation, the non-polar tail of the DDA enabled the RuO_2 particles to disperse easily in non-polar organic solvents, such as toluene or hexane.

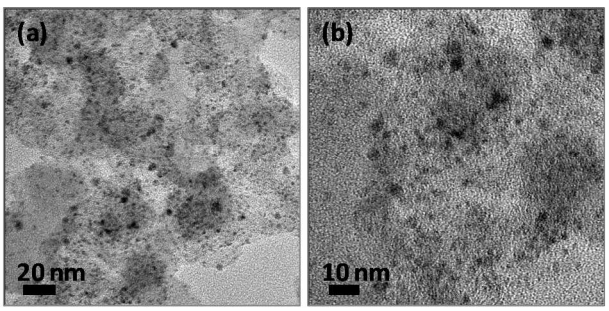

Fig. 1 TEM (a) and HRTEM images (b) of RuO_2/C nanocomposites as-prepared by a solvothermal approach.

After aging the mixture of RuO_2 nanoparticles in toluene and

XC-72 carbon supports under vigorous stirring for 4 h at room temperature, the RuO_2 nanoparticles could be efficiently loaded on the carbon supports, leading to the formation of RuO_2/C nanocomposites and leaving behind a clear toluene phase. The representative TEM and HRTEM images in Fig. 1 show that the RuO_2 nanoparticles with spherical morphology are dispersed very well on the carbon supports. As indicated by the histogram in Fig. S1 of Electronic Supplementary Information (ESI), these RuO_2 nanoparticles in the RuO_2/C nanocomposites are nearly mono-dispersed, and have an average size of 1.8 nm. The low and broad diffraction peaks displayed in the XRD pattern shown in Fig. 2 are from the carbon supports in the RuO_2/C nanocomposites, and no crystalline RuO_2 diffraction peaks are observed, demonstrating the formation of amorphous RuO_2 phase.

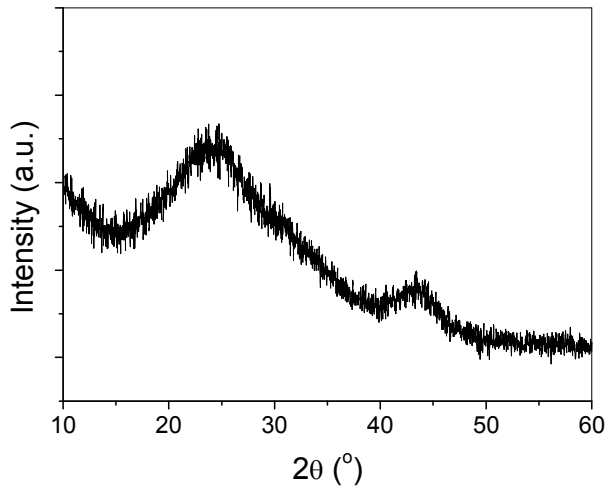

Fig. 2 The X-ray diffraction (XRD) pattern of RuO_2/C nanocomposites as-prepared by a solvothermal approach.

The Ru in RuO_2/C nanocomposites was examined by XPS to confirm its chemical state. Unfortunately, the Ru $3d_{3/2}$ peak overlaps with the C 1*s* peak, preventing an unambiguous analysis of the nanoparticle surface. Therefore, the Ru 3p peak was used instead. As shown in Fig. 3, one doublet at 462.5 and 484.8 eV, which reflects the Ru at oxidized state, e.g. RuO_2,[28–30] can fit for the XPS spectrum very well. indicating that the RuO_2 was the dominant product upon the decomposition of $RuCl_3$-DDA complexes at elevated temperature in air.

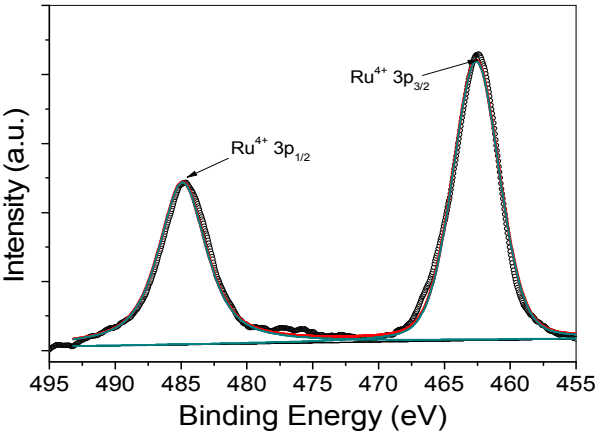

Fig. 3 3p XPS spectrum of Ru in RuO_2/C nanocomposites as-prepared by a solvothermal approach.

3.2 RuO_2-Au/C nanocomposites

In the absence of carbon supports, the mixture of $RuCl_3$ and $HAuCl_4$ with Ru/Au molar ratio of 3:1 would be completely precipitated after heating at 110°C for 5 min, leaving behind a clearly aqueous solution. A typical EDX analysis shown in ESI Fig. S2 for the precipitates shows that the ratio of Ru to Au is ca. 3:1 in the precipitates. XPS was also used to analyze the state of precipitates. Fig. 4a and b show the spectra of Ru 3p region and Au 4f region, respectively. The Ru 3p XPS signal could be fitted very well by one doublet at 462.5 and 484.8 eV, which corresponds to the Ru^{4+}, e.g RuO_2.[28–30] In Au 4f region, the doublet in XPS spectra at 83.8 and 87.5 eV is a signature of Au metal in the zero valent state.[28] XPS analyses show that the main components in the precipitates obtained from the mixture of $RuCl_3$ and $HAuCl_4$ are RuO_2 and metallic Au.

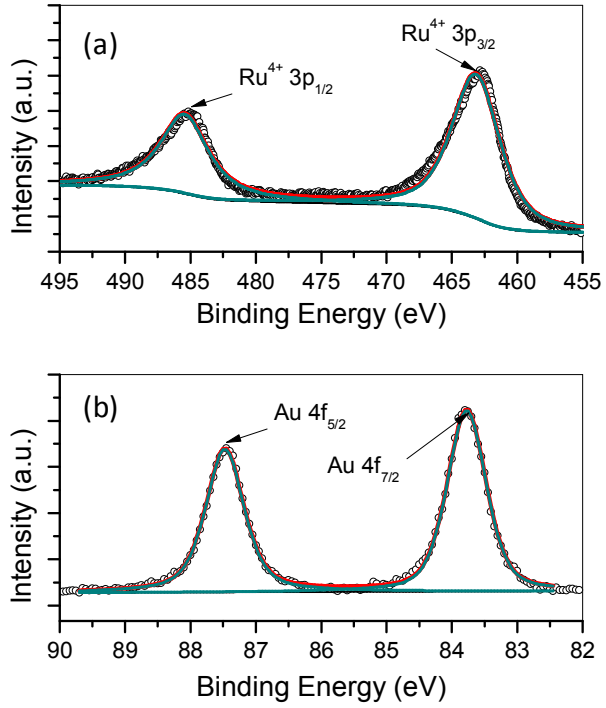

Fig. 4 3p XPS spectrum of Ru (a) and 4f XPS spectrum of Au (b) in RuO_2-Au/C nanocomposites as-prepared by a mutual oxidation-reduction approach.

Then the following reaction mechanism was put forward, which well rationalizes the analyses resulted from EDX and XPS:

$$3RuCl_3 + HAuCl_4 + 6H_2O \rightarrow 3RuO_2 + Au + 13HCl$$

In this mechanism, ions of Ru^{3+} in $RuCl_3$ are further oxidized to Ru^{4+} by $HAuCl_4$, while the Au^{3+} ions in $HAuCl_4$ were reduced to metallic Au at zero valent state. $RuCl_3$ and $HAuCl_4$ serve as reducing and oxidizing agent, respectively, for each other. The mechanism above is not only satisfied with the EDX and XPS

analyses but also interprets convincingly the complete precipitates in the mixture of $RuCl_3$ and $HAuCl_4$ with molar ratio of 3:1, in which the original ratio of Ru to Au is fit for the composition in the final reaction product and thus complete precipitation is induced.

When XC-72 carbon supports were introduced before heating, nanocomposites composed of bimetallic RuO_2-Au nanoparticles and carbon were formed instead of precipitates. TEM and HRTEM images of the nanocomposites were shown in Fig. 5a and b, respectively. As exhibited, the bimetallic RuO_2-Au particles in the RuO_2-Au/C nanocomposites, which are quite small (average particle size of 1.62 nm) and the particle size distribution is very narrow (relative standard deviation of 14.8%, as seen in ESI Fig. S3), are uniformly distributed on the carbon supports. Again, EDX analyses on several random areas in TEM grid show that the composition is very uniform, in accord with the 3:1 ratio of Ru to Au very well, which rules out the formation of physical mixture of isolated RuO_2 and Au particles. In addition, in XRD pattern, as shown in Fig. 6, only Au with face-centered cubic (fcc) phase is observed (JCPDF Card File 893697), indicating the amorphous feature of RuO_2 in RuO_2-Au/C nanocomposites.

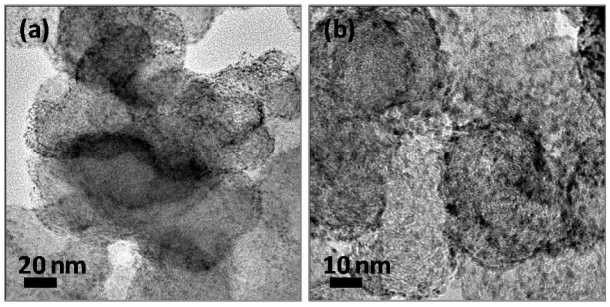

Fig. 5 TEM (a) and HRTEM images (b) of RuO_2-Au/C nanocomposites as-prepared by a mutual oxidation-reduction approach.

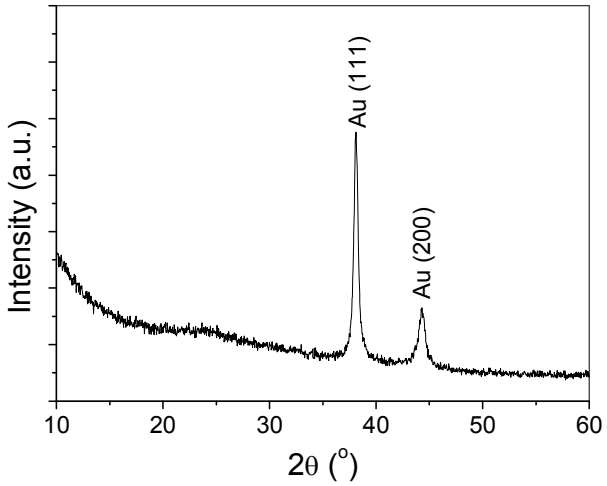

Fig. 6 The X-ray diffraction (XRD) pattern of RuO_2-Au/C nanocomposites as-prepared by a mutual oxidation-reduction approach.

3.3 Electrochemical properties of RuO_2/C and RuO_2-Au/C nanocomposites

Transition metal oxides are considered to be the best candidate materials for supercapacitors because of their high specific capacitance coupled with very low resistance resulting in a high specific power, which renders them very appealing in commercial applications.[31,32] Among the transition metal oxides, RuO_2 in either a crystalline or amorphous hydrous form is the most promising electrode material due to its high specific capacitance, long cycle life, high conductivity, and good electrochemical reversibility, as well as its high rate capability.[33–37] Currently, the research efforts focus on RuO_2-based compounds providing high cyclability and capacitance.[38–41]

The RuO_2/C and RuO_2-Au/C nanocomposites synthesized in this work were examined for their electrochemical properties as supercapacitor materials. Fig. 7a and b exhibit the CV curve of RuO_2/C and RuO_2-Au/C nanocomposites measured in 1 M H_2SO_4 with a potential range of -1~1 V at scan rates of 10, 20, 50 and 100 mV s^{-1}, respectively. Observed from the tested CV curves, the rectangle shapes suggest good capacitive behavior for the RuO_2/C and RuO_2-Au/C nanocomposites. Furthermore, this rectangular CV curves do not change distinctly with the increase of scan rates, demonstrating a satisfied electrical conductivity of the electrode material. In the case of RuO_2-Au/C nanocomposites, a higher current of electrochemical response is observed from Fig. 7b. The CV curves of RuO_2-Au/C nanocomposites (Fig. 7b) exhibit more rectangular shape compared with that of RuO_2/C nanocomposites (Fig. 7a), revealing that the RuO_2-Au/C nanocomposites have better capacitive behavior than that of RuO_2/C nanocomposites. The presence of gold in RuO_2-Au/C nanocomposites would be favorable for the electronic/ionic conductivity, and may account for the enhancement in capacitive behavior of RuO_2.[42]

Fig. 7c and d displays the galvanostatic charge–discharge curves of the RuO_2/C and RuO_2-Au/C nanocomposites, respectively, at different current densities. The almost triangular shape indicates its ideal capacitive behavior because of the high degree of symmetry in charge and discharge. The specific capacitance of RuO_2/C nanocomposites is 537.7, 394.1, 350.1, and 315.8 F g^{-1} at current densities of 50, 100, 200 and 500 mA g^{-1}, respectively, as shown in Fig. 7e. While for RuO_2-Au/C nanocomposites, the specific capacitances at current densities of 50, 100, 200 and 500 mA g^{-1} are 558.2, 514.5, 478.5, and 458.5 F g^{-1}, respectively, as shown in Fig. 7f. As a typical example, the comparison of the specific capacitances of RuO_2/C and RuO_2-Au/C nanocomposites at current density of 200 mA g^{-1} was illustrated in Fig. 7g, which clearly supports that the RuO_2-Au/C nanocomposites has higher specific capacitance than that of RuO_2/C nanocomposites, suggesting that the presence of Au in the nanocomposites has positive effect on the capacitive behavior of RuO_2 when the weight of only RuO_2 in the nanocomposites is used to calculate.

The specific power density (P) and energy density (E) were calculated using the following equations:

$$P = \frac{V^2}{4mR}; \quad E = CV^2/2$$

where P and E are the specific power density (kW kg^{-1}) and energy density (Wh kg^{-1}), respectively; V is the maximum potential (V), R is the equivalent series resistance (Ω); m is the

mass of the electro-active materials in the capacitor (g); and C is the specific capacitance (F g^{-1}). In this article, the equivalent series resistances of the capacitors consisted of RuO_2-Au/C and RuO_2/C materials are 0.66 Ω and 1.1 Ω, respectively. Calculations by the equations above indicate that the P and E for the RuO_2/C-based capacitor are 56.8 kW kg^{-1} and 43.9 Wh kg^{-1}, while for RuO_2-Au/C-based capacitor are 95.1kW kg^{-1} and 63.7 Wh kg^{-1}, respectively.

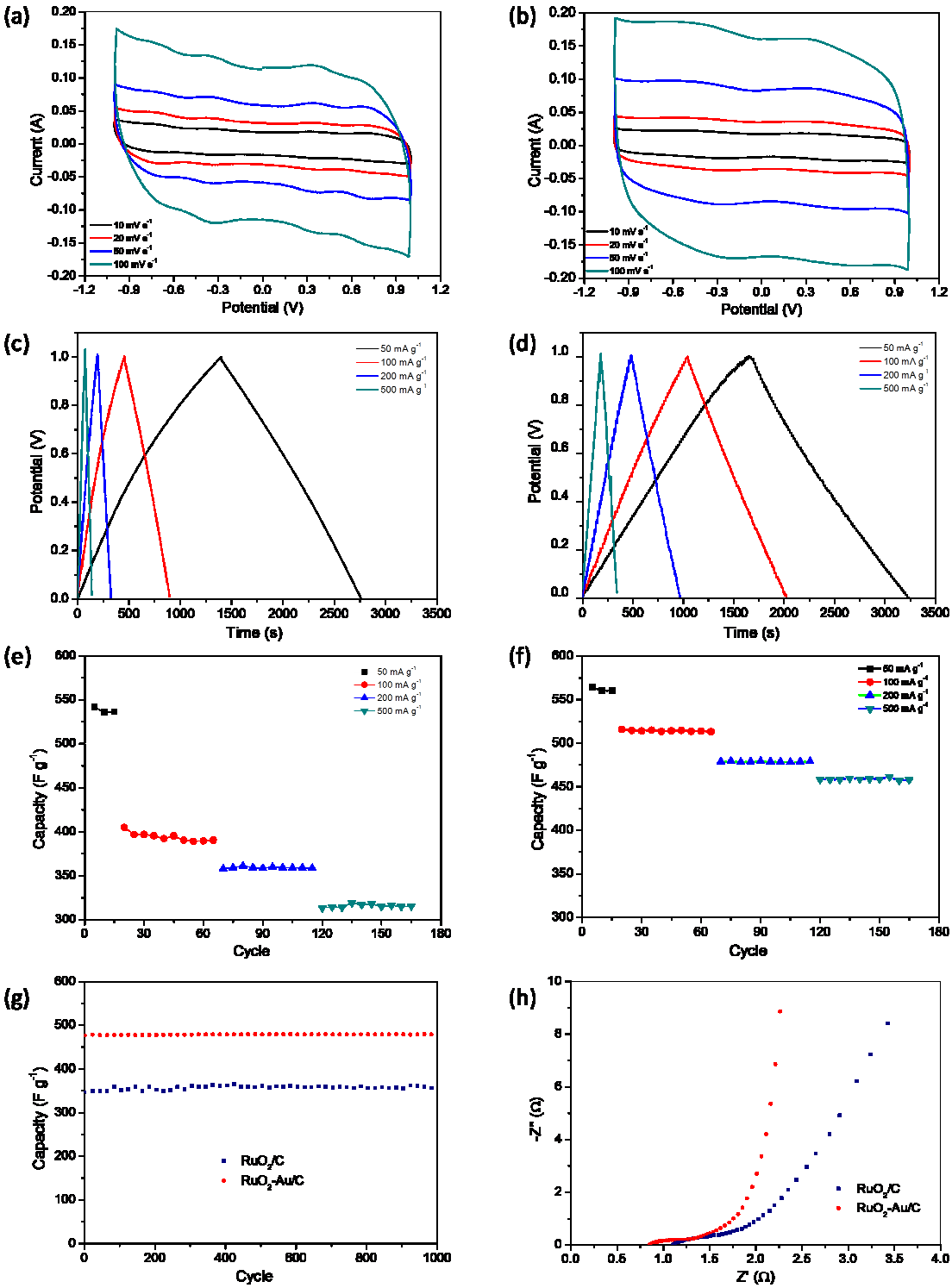

Fig. 7 Cyclic voltammograms of RuO_2/C (a) and RuO_2-Au/C nanocomposites (b) at different scan rates; galvanostatic charge-discharge curves of RuO_2/C (c) and RuO_2-Au/C nanocomposites (d) at different current densities; plots of specific capacitance for RuO_2/C (e) and RuO_2-Au/C nanocomposites (f) at different current densities; comparison of the specific capacitance for RuO_2/C and RuO_2-Au/C nanocomposites at current density of 200 mA g^{-1} (g); comparison of Nyquist plots for RuO_2/C and RuO_2-Au/C nanocomposites (h).

Fig. 7h shows the Nyquist plots of the RuO_2/C and RuO_2-Au/C nanocomposites measured by electrochemical impedance spectroscopy (EIS), which illustrate the frequency response of the electrode/electrolyte system. The more vertical the curve, the more closely the supercapacitor behaves as an ideal capacitor. As shown in the Nyquist plots, in the low-frequency area the curve of RuO_2-Au/C nanocomposites is more vertical to the *x* axis than that of RuO_2/C nanocomposites, indicating a significant enhancement of the electron–proton transport in RuO_2-Au/C nanocomposites. In the high-frequency area, the interception of the curve in the real part *Z*' indicates the bulk resistance of the electrochemical system. Again, the RuO_2-Au/C nanocomposites display very low bulk resistance.

4 Conclusions

In summary, we reported a solvothermal strategy and a mutual oxidation-reduction approach for the fabrication of RuO_2-based nanocomposites, including RuO_2/C and RuO_2-Au/C. The syntheses were based on a thermal decomposition of metal complexes formed by $RuCl_3$ and dodecylamine at room temperature (for RuO_2/C) and the mutual oxidation-reduction phenomenon between $RuCl_3$ and $HAuCl_4$ at elevated temperature (for RuO_2-Au/C) in the presence of carbon supports. The as-prepared RuO_2/C and RuO_2-Au/C nanocomposites for supercapacitor adopting the H_2SO_4 electrolyte exhibit high specific capacitances of 537.7 F g^{-1} and 558.2 F g^{-1}, respectively, at a current density of 50 mA g^{-1}. The specific capacitance maintains 350.1 F g^{-1} for RuO_2/C nanocomposites and 478.5 F g^{-1} for RuO_2-Au/C nanocomposites at current density of 200 mA g^{-1} with good cycling stability. The comparison of the electrochemical measurements of RuO_2/C and RuO_2-Au/C nanocomposites demonstrates that the presence of Au in the nanocomposites is favorable for the enhancement in capacitive behavior of RuO_2 by increasing its electronic/ionic conductivity. The remarkable simplicity may render the approaches developed in this work promising for creating RuO_2-based nanomaterials on a large scale for supercapacitor applications.

Aknowledgement

Financial support from the Knowledge Innovation Program of the Chinese Academy of Sciences (Grant No. KGCX2-YW-341), the 100 Talents Program of the Chinese Academy of Sciences, National Natural Science Foundation of China (Grant No.: 21173226, 21376247), and State Key Laboratory of Multiphase Complex Systems, Institute of Process Engineering, Chinese Academy of Sciences (MPCS-2012-A-11) is gratefully acknowledged.

Notes and references

[a] *State Key Laboratory of Multiphase Complex Systems, Institute of Process Engineering, Chinese Academy of Sciences, Beijing, China 100190. Tel.: 86-10-6252 9377; Fax: 86-10-8254 5008; E-mail: qtan@ipe.ac.cn (Q.T.); Fax: 86-10-8254 4814; Tel: 86-10-8254 4915; E-mail: jyang@mail.ipe.ac.cn (J.Y.)*

[b] *University of Chinese Academy of Sciences, No. 19A Yuquan Road, Beijing, China 100049*

†Electronic Supplementary Information (ESI) available: Additional Histograms and EDX analysis for the characterization of the nanostructures in this study. See DOI:10.1039/b000000x/

1 T. Mokari, E. Rothenberg, I. Popov, R. Costi and U. Banin, *Science*, 2004, **304**, 1787.
2 H. Yu, M. Chen, P. M. Rice, S. X. Wang, R. L. White and S. Sun, *Nano Lett.*, 205, **5**, 379.
3 W. L. Shi, H. Zeng, Y. Sahoo, T. Y. Ohulchanskyy, Y. Ding, Z. L. Wang, M. Swihart and P. N. Prasad, *Nano Lett.*, 2006, **6**, 875.
4 J. Yang, H. I. Elim, Q. B. Zhang, J. Y. Lee and W. Ji, *J. Am. Chem. Soc.*, 2006, **128**, 11921.
5 D. V. Talapin, H. Yu, E. V. Shevchenko, A. Lobo and C. B. Murray, *J. Phys. Chem. C*, 2007, **111**, 14049.
6 A. Figuerola, A. Fiore, R. D. Corato, A. Falqui, C. Giannini, E. Micotti, A. Lascialfari, M. Corti, R. Cingolani, T. Pellegrino, P. D. Cozzoli and L. Manna, *J. Am. Chem. Soc.*, 2008, **130**, 1477.
7 J. Yang and J. Y. Ying, *Chem. Commun.*, 2009, 3187.
8 J. Zhang, X. H. Liu, X. Z. Guo, S. H. Wu and S. R. Wang, *Chem. Eur. J.*, 2010, **16**, 8108.
9 S. Huang, J. Huang, J. Yang, J.-J. Peng, Q. Zhang, F. Peng, H. Wang and H. Yu, *Chem. Eur. J.*, 2010, **16**, 5920.
10 L. Carbone and P.D. Cozzoli, *Nano Today*, 2010, **5**, 449.
11 J. Yang, J. Y. Lee and J. Y. Ying, *Chem. Soc. Rev.*, 2011, **40**, 1672.
12 W. Hu, H. Liu, F. Ye, Y. Ding and J. Yang, *CrystEngComm*, 2012, **14**, 7049.
13 M. R. Buck, J. F. Bondi and R. E. Schaak, *Nat. Chem.*, 2012, **4**, 37.
14 H. Liu, F. Ye, H. Cao, G. Ji, J. Y. Lee amd J. Yang, *Nanoscale*, 2013, **5**, 6901.
15 Y. Li, Q. Zhang, A. V. Nurmikko and S. Sun, *Nano Lett.*, 2005, **5**, 1689.
16 J. Jiang, H. Gu, H. Shao, E. Devlin, G. C. Papaefthymiou and J. Y. Ying, *Adv. Mater.*, 2008, **20**, 4403.
17 R. Costi, A. E. Saunders, E. Elmalem, A. Salant and U. Banin, *Nano Lett.*, 2008, *8*, 637.
18 J. S. Lee, E. V. Shevchenko and D. V. Talapin, *J. Am. Chem. Soc.*, 2008, **130**, 9673.
19 J. M. Zhu, Y. H. Shen, A. J. Xie and L. Zhu, *J. Mater. Chem.*, 2008, **19**, 8871.
20 C. Wang, H. Yin, S. Dai and S. Sun, *Chem. Mater.*, 2010, **22**, 3277.
21 L. Zhang, D. A. Blom and H. Wang, *Chem. Mater.*, 2011, **23**, 4587.
22 J. Yang and J. Y. Ying, *Angew. Chem. Int. Ed.*, 2011, **50**, 4637.
23 X. Sun, S. Guo, Y. Liu and S. Sun, *Nano Lett.*, 2012, **12**, 4859.
24 X. Ding, Y. Zou, F. Ye, J. Yang and J. Jiang, *J. Mater. Chem. A*, 2013, **1**, 11880.
25 C. Wang, H. Daimon and S. Sun, *Nano Lett.*, 2009, **9**, 1493.
26 J. Yang, X. Chen, F. Ye, C. Wang, Y. Zheng and J. Yang, *J. Mater. Chem.*, 2011, **21**, 9088.
27 J. Yang, E. H. Sargent, S. O. Kelley and J. Y. Ying, *Nat. Mater.*, 2009, **8**, 683.
28 C. D. Wagner, A. V. Naumkin, A. Kraut-Vass, J. W. Allison, C. J. Powell and J. R. Rumble, *NIST Standard Reference Database 20*, Version 3.2 (Web version).
29 Z. Liu, J. Y. Lee, M. Han, W. X. Chen and L. M. Gan, *J. Mater. Chem.*, 2002, **12**, 2453.
30 X. Zhang and K.-Y. Chan, *Chem. Mater.*, 2003, **15**, 451.
31 Y. Zhang, H. Feng, X. Wu, L. Wang, A. Zhang, T. Xia, H. Dong, X. Li and L. Zhang, *Int. J. Hydrogen Energy*, 2009, **34**, 4889.
32 C. D. Lokhande, D. P. Dubal and O.-S. Joo, *Curr. Appl. Phys.*, 2011, **11**, 255.
33 I.-H. Kim and K.-B. Kim, *J. Electrochem. Soc.*, 2006, **153**, A383.
34 C.-Y. Lee and A.M. Bond, *Langmuir*, 2010, **26**, 16155.
35 K. M. Kim, J. H. Nam, Y.-G. Lee, W. I. Cho and J. M. Ko, *Curr. Appl. Phys.*, 2013, **13**, 1702.
36 Z. Zhou, Y. Zhu, Z. Wu, F. Lu, M. Jing and X. Ji, *RSC Adv.*, 2014, **4**, 6927.
37 N. Kang, T. Yu, G.-H. Lim, T. Koh and B. Lim, *Chem. Phys. Lett.*, 2014, **592**, 192.
38 Y.-F. Su, F. Wu, L.-Y. Bao and Z.-H. Yang, *New Carbon Mater.*, 2007, **22**, 53.
39 H. Xia, Y. S. Meng, G. Yuan, C. Cui and L. Lu, *Electrochem. Solid-State Lett.*, 2012, **15**, A60.

40 H.-T. Fang, M. Liu, D.-W. Wang, X.-H. Ren and X. Sun, *Nano Energy*, 2013, **2**, 1232.
41 R. B. Rakhi, W. Chen, M. N. Hedhili, D. Cha and H. N. Alshareef, *ACS Appl. Mater. Interfaces*, 2014, **6**, 4196.
42 L. Y. Chen, Y. Hou, J. L. Kang, A. Hirata, T. Fujita and M. W. Chen, *Adv. Energy Mater.*, 2013, **3**, 851.

Graphical abstract

Ruthenium oxide-based nanocomposites with high specific surface area and improved capacitance as a supercapacitor

Pengfei Wang,[ab] Hui Liu,[a] Qiangqiang Tan[a]* and Jun Yang[a]*

A solvothermal approach and a mutual oxidation-reduction strategy were demonstrated for the synthesis of RuO_2-based nanocomposites for supercapacitors.